Geophysical Research Letters

RESEARCH LETTER
10.1029/2025GL115228

Inefficient Melt Transport Across a Weakened Lithosphere Led to Anomalous Rift Architecture in the Turkana Depression

Adina E. Pusok[1], Yuan Li[1], Tim Davis[1,2], Dave A. May[3], and Richard F. Katz[1]

[1]Department of Earth Sciences, University of Oxford, Oxford, UK, [2]School of Earth Sciences, University of Bristol, Bristol, UK, [3]Scripps Institution of Oceanography, San Diego, CA, USA

Key Points:

- Two-phase flow models show that melt transport across a thin, weakened lithosphere is slower than across a thick, elastic lithosphere
- Extension is accommodated by both magmatic intrusion and distributed fault slip in a thin, weakened lithosphere
- The widespread faulting and magmatism in the Turkana Depression can be explained by a history of lithospheric thinning and weakening

Supporting Information:

Supporting Information may be found in the online version of this article.

Correspondence to:

A. E. Pusok,
adina.pusok@earth.ox.ac.uk

Citation:

Pusok, A. E., Li, Y., Davis, T., May, D. A., & Katz, R. F. (2025). Inefficient melt transport across a weakened lithosphere led to anomalous rift architecture in the Turkana Depression. *Geophysical Research Letters*, *52*, e2025GL115228. https://doi.org/10.1029/2025GL115228

Received 10 FEB 2025
Accepted 1 MAY 2025

Author Contributions:

Conceptualization: Adina E. Pusok
Formal analysis: Adina E. Pusok, Yuan Li
Funding acquisition: Adina E. Pusok, Richard F. Katz
Investigation: Adina E. Pusok, Yuan Li, Tim Davis, Richard F. Katz
Methodology: Adina E. Pusok, Yuan Li, Tim Davis, Richard F. Katz
Project administration: Adina E. Pusok, Richard F. Katz
Resources: Adina E. Pusok, Richard F. Katz
Software: Adina E. Pusok, Yuan Li, Dave A. May
Validation: Adina E. Pusok, Tim Davis, Richard F. Katz

Abstract The Turkana Depression, located between the Ethiopian and East African plateaus, displays an anomalous rift architecture. It is missing the narrow, magma-rich morphology observed in the Main Ethiopian Rift that cuts through the Ethiopian Plateau. Instead, diffuse faulting and isolated volcanic centers are widespread over several hundred kilometers. Turkana has also experienced less magmatism over the last 30 Myr than adjacent plateaus, despite having a thin crust and residing above a mantle that is inferred to be hot and partially molten. We hypothesize that lithospheric weakening has been the key control on magma transport across the lithosphere in the Turkana Depression and subsequent rift development. Using poro-viscoelastic–viscoplastic models of melt transport, we show that magma extraction across a thin, weakened lithosphere is slower than across a thick, elastic lithosphere. Our results suggest that pre-rift lithospheric strength can explain the magma-poor character of Turkana for most of its tectonic history.

Plain Language Summary A continental rift is a nascent plate tectonic boundary where a continent splits apart. The East African Rift system is the most comprehensively studied active continental rift on our planet, yet how magmatism and tectonics interact along the roughly 5,000-km-long system remains unclear. After an extensive outpouring of magma ~30 million years ago that led to the formation of the Ethiopian and East African plateaus, both magmatism and faulting localized in the interior of these plateaus in narrow, fault-bounded valleys such as the Main Ethiopian Rift. However, the rift architecture in the Turkana Depression, south of the Ethiopian Plateau, is in marked contrast to its neighbors': faulting and magmatism are widespread over several hundred kilometers. We propose here that the complex rifting history in Turkana rendered the lithosphere thin and weak, which acted as a barrier to melt pathways from depth to the surface. Using numerical models of melt transport that capture porous flow and fluid-driven fracture, we show a counter-intuitive relationship between lithospheric strength, thickness, and melt extraction. We suggest this relationship can explain the deformation pattern in the Turkana Depression, and has implications toward understanding the coupled magmatic–tectonic history of rifting.

1. Introduction

The East African Rift system developed above a deep-seated, buoyant mantle plume in the last 30 Myr (e.g., Ebinger & Sleep, 1998; Kendall & Lithgow-Bertelloni, 2016; Moucha & Forte, 2011). The upwelling flow and associated magmatism provided the heat and extensional stresses necessary to weaken and break the continental lithosphere (Bialas et al., 2010; Buck, 2006; Buck et al., 2004; Kendall & Lithgow-Bertelloni, 2016; Rajaonarison et al., 2023; Stamps et al., 2014). The main phase of flood-basalt volcanism between 32 and 25 Ma led to the formation of the Ethiopian and East African Plateaus (Figure 1a, e.g., Corti, 2009; Courtillot et al., 1999; Ebinger et al., 1989). After the onset of rifting in the northern part of the rift system at ~25 Ma (Ebinger et al., 2000; Morley et al., 1992), magmatism and extension localized toward the interior of these plateaus, developing narrow, magma-rich rift valleys in the last 10 Myr (e.g., Brune et al., 2023; Ebinger & Casey, 2001; Rooney, 2020). Geophysical studies along the Main Ethiopian Rift (MER) and Eastern Rift confirm that their fault-bounded, 60–100-km-wide basins accommodate extension mostly by magmatic intrusion (Bastow et al., 2010; Chambers et al., 2022; Cornwell et al., 2006; Ebinger & Casey, 2001; Erbello et al., 2024; Kendall et al., 2006; Oliva et al., 2019; Tiberi et al., 2019). In contrast, the Turkana Depression is missing the rift-valley morphology; instead, faulting, seismicity, and volcanic centers are widespread over several hundred kilometers across the region (Ebinger et al., 2000; Morley et al., 1992). Extension in Turkana has been accommodated largely by

Visualization: Adina E. Pusok
Writing – original draft: Adina E. Pusok
Writing – review & editing: Adina E. Pusok, Yuan Li, Tim Davis, Dave A. May, Richard F. Katz

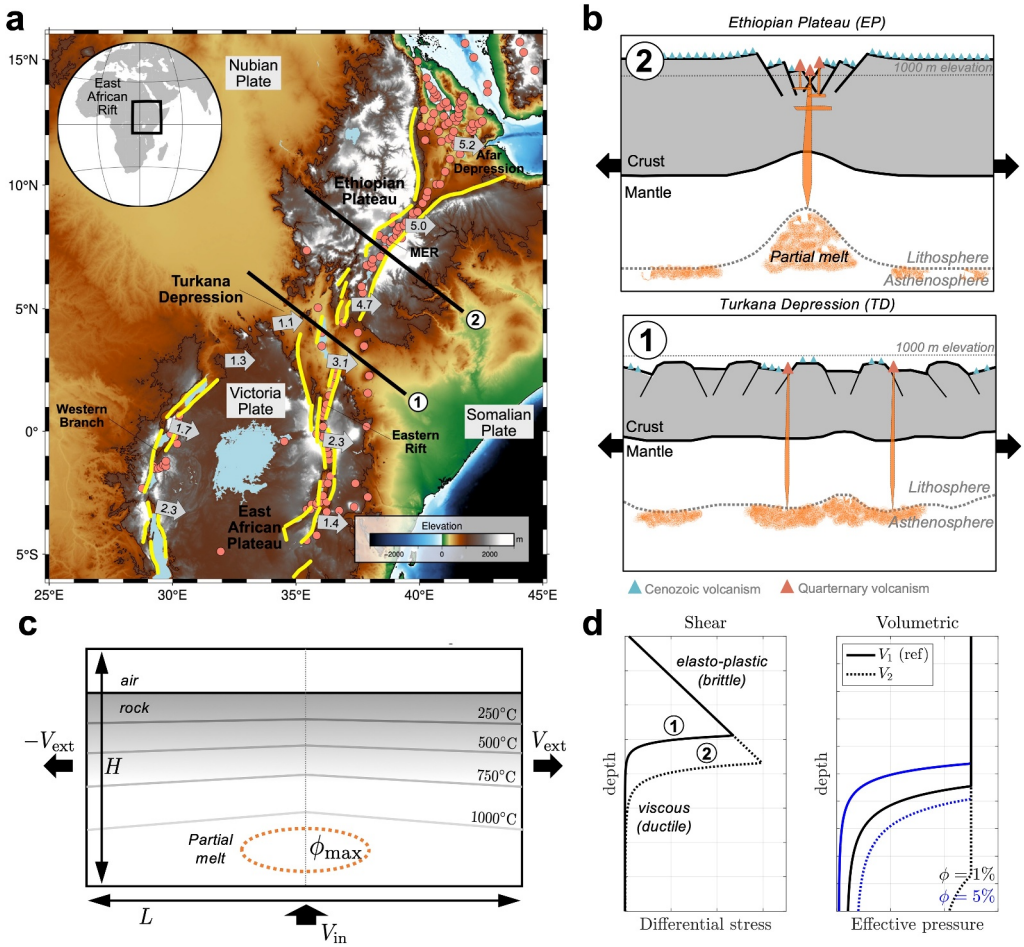

Figure 1. (a) Tectonic setting of the northern part of the East African Rift. Yellow lines are fault traces; pink circles are Quaternary volcanoes (Global Volcanism Program, 2013; Kounoudis et al., 2021); gray arrows show motion relative to a stable Nubian plate, with values in mm/yr (Knappe et al., 2020; Saria et al., 2014). MER: Main Ethiopian Rift. (b) Schematic cross-sections across the Turkana Depression (1) and the Ethiopian Plateau (2). (c) Numerical model set-up for a section of lithosphere under extension, with kinematic boundary conditions on the side boundaries. V_{ext} is extension rate and L, H are domain length and height. The background strain rate is calculated as $\dot{\epsilon}_{BG} = 2V_{\text{ext}}/L$. The temperature field is initialized with a half-space cooling model, which determines the lithospheric strength. An initial magma body is prescribed with a Gaussian porosity distribution, where $\phi_{\max}$ is the maximum amplitude. (d) Strength–depth profiles for shear and volumetric (isotropic) deformation, calculated for given temperature distribution and background strain rates (see Supporting Information S1). Shear strength: (1) solid line corresponds to a case with a thin brittle layer and small Maxwell time ($t_{\text{M}}^{\text{shear}} = \eta/G$, where η is shear viscosity and G is shear modulus), (2) dotted line corresponds to a case with a thick brittle layer and high Maxwell time. Volumetric strength: similar as for shear (i.e., $t_{\text{M}}^{\text{vol}} = \zeta/Z$, where ζ is compaction viscosity and Z is bulk modulus). Magma has a weakening effect on both shear and volumetric strengths illustrated by the blue lines, where ϕ is porosity or the volume fraction of magma. All parameters and units are detailed in Table A2 in Supporting Information S1.

faulting and stretching, rather than dike intrusion, until the last 1 Myr (Morley, 2020; Muirhead et al., 2022; Rooney et al., 2022).

Various hypotheses have been advanced to explain the contrast between Turkana and the Ethiopian Plateau/MER. Some geochemical and geodynamical modeling studies proposed that multiple plumes exist beneath East Africa (Furman et al., 2006; George et al., 1998; Lin et al., 2005; Rogers et al., 2000), such that Turkana formed above a gap between plumes and has had less dynamic mantle support (Benoit et al., 2006; Mechie et al., 1994). This idea has been challenged in favor of a single, possibly heterogeneous, plume hypothesis (Ebinger & Sleep, 1998; Rooney et al., 2012). Global (Boyce et al., 2021; Ritsema et al., 2011) and regional (Kounoudis et al., 2021) seismic imaging shows that both the Turkana Depression and the uplifted plateaus are underlain by hot, partially molten, buoyant mantle. More recently, the low elevation in Turkana has been attributed to crustal thinning

(Benoit et al., 2006; Ogden et al., 2023). The Turkana Depression has among the thinnest crust and highest crustal-stretching factors along the East African Rift system south of Afar, with crustal thickness estimated to be 10–20 km less than surrounding plateaus, where it is ∼35–40 km (Benoit et al., 2006; Mechie et al., 1994, 1997; Ogden et al., 2023) (Figure 1b, profiles 1 and 2).

The Turkana Depression also has a distinct tectonic and magmatic history relative to the neighboring regions. Prior to plume-related magmatism, Turkana experienced two rifting episodes during the Cretaceous (130–80 Ma) and Paleogene (66–50 Ma) thought to have thinned and weakened the lithosphere (Boone et al., 2018; Ebinger & Ibrahim, 1994; Ebinger et al., 2000; Morley et al., 1992). The earliest Cenozoic flood basalt magmatism also began in the northern part of Turkana and SW Ethiopia (∼45–35 Ma, Davidson & Rex, 1980; George et al., 1998; Pik et al., 2006), but reached only as far south as ∼5.5°N to the east of Lake Turkana (Rooney, 2017; Steiner et al., 2022). This early magmatic episode did not, however, result in Turkana progressing rapidly to a magma-rich system like the MER. Instead, sporadic phases of volcanism with 5–7 Myr hiatuses span the last 30 Myr (Muirhead et al., 2022; Rooney, 2020; Rooney et al., 2022; Steiner et al., 2022). Miocene–recent rifting in Turkana has been neither magma-rich like the MER, nor entirely magma-poor. A common presumption seems to be that the difference between magma-poor and magma-rich architecture reflects different stages of rifting, where the strain is increasingly accommodated by magmatism as a rift system matures (Brune et al., 2023; Corti, 2009; Ebinger & Casey, 2001). This hypothesis predicts increasing volcanism with progressive thinning of the lithosphere, and therefore it predicts that the Turkana Depression should have experienced more volcanism or developed earlier into a magma-rich rift. It thus remains unclear how diffuse magmatism and deformation evolved in this region of extremely thin crust and with a persistent mantle plume source.

Previous rift modeling suggests that a weakened lithosphere, as a result of thermal or mechanical weakening, can produce a pattern of diffuse deformation (e.g., Brune et al., 2017; Buck, 1991). Early models showed that thermal weakening due to magmatic intrusion may explain variations in rift faulting; hot, weak lithosphere develops broad rift zones bounded by low-angle border faults, while cold, strong lithosphere develops narrow rift zones bounded by high-angle border faults (Buck, 1991). In Turkana, the crustal thinning and broadly distributed deformation have been attributed to lithospheric weakness inherited as damage from multiple rifting episodes (Ebinger & Ibrahim, 1994; Hendrie et al., 1994; Morley, 1994, 1999; Morley et al., 1992). Analog and numerical models support the hypothesis that inherited heterogeneities from the Mesozoic rifting may explain the transition from narrow rifting in Ethiopia and Kenya to distributed deformation within Turkana (Brune et al., 2017; Corti et al., 2019). However, these models have neglected the effects of magmatism and cannot explain the unusual relationship between crustal thinning, faulting, and magmatism observed in Turkana. Here, we hypothesize that lithosphere thinning and weakening in the Turkana Depression has influenced magma transport across the lithosphere and subsequent rift development over the last 30 Myr. Using new models of melt transport across the brittle–ductile transition, we investigate how magma traverses the lithosphere of varying strengths in a tectonic setting similar to Turkana and the Ethiopian Plateau prior to and at early stages of Miocene–recent rifting. Results show that magma extraction across a thin, weakened lithosphere is slower than across a thick, elastic lithosphere. We argue that this difference in vertical extraction rates explains the pattern of magmatism and faulting in the Turkana region relative to the Ethiopian Plateau/MER.

2. Models of Magma Extraction Across the Ductile–Brittle Lithosphere

We test the hypothesized scenario with numerical models of magma transport across the ductile–brittle transition (see Supporting Information S1 for detailed methods). We solve for conservation of mass, momentum, and energy for a two-phase system, rock and magma, with a poro-viscoelastic–viscoplastic rheological law and a free surface (Li et al., 2023, 2025; Pusok et al., 2022). The model domain is a cross-section of the lithosphere under extension (Figure 1c). The rheological formulation and thermal structure together reproduce the transition from an elastic–brittle layer to a ductile layer with depth (Figure 1d). Brittle deformation is modeled using a plastic failure envelope that approximates the Griffith and Drucker-Prager yield criteria for tensile and shear failure, respectively. When the porosity (ϕ) is above a small threshold value ($\phi_{Tz} = 10^{-4}$), the stresses used to test for plastic failure are modified according to Terzaghi's law (Terzaghi, 1943), which states that the fluid pressure may assist in the formation of fractures. This threshold plays a prominent role in the dynamics and will be discussed below. Models are initialized with an imposed source of partial melt at depth, which rises due to its buoyancy. Melting and crystallization are excluded, such that we cannot distinguish between mantle- or crustal-derived melts during

rifting; instead, we focus on something neglected by previous studies: the impact of lithospheric rheology on magma transport.

The modeled tectonic scenario is similar to the Turkana Depression and Ethiopian Plateau prior to and at early stages of rifting ~30 Myr, in which the Turkana lithosphere has already been thinned and weakened. We assume that the factors controlling rifting and magmatism, such as the forces driving rifting and the mantle plume source, after this age affected both regions equivalently. The model setup, therefore, represents a cross-section of the lithosphere and captures the first-order regional tectonic features of the Turkana Depression and the Ethiopian Plateau (Figure 1c). The strength of the lithosphere is conceptualized with simple brittle–ductile yield strength envelopes, which are typically used to investigate rift dynamics (e.g., Brune et al., 2023) and interpret crustal seismicity (Albaric et al., 2009). The contrast in lithospheric strength between the Turkana Depression and the Ethiopian Plateau is captured in our models as a difference of 5–10 km in the brittle-layer thickness (Figure 1d, shear strength profiles 1, 2). Turkana has a shallow brittle–ductile transition, while the region of Ethiopian Plateau has a deeper transition. A more complex rheological structure of the lithosphere may be chosen, but it would obscure our understanding of the model results and could be at odds with tectonic reconstructions. Instead, this rheological contrast is consistent with present-day seismic (Albaric et al., 2009; Craig & Jackson, 2021; Musila et al., 2023; Ogden et al., 2023) and elastic thickness estimates (Pérez-Gussinyé et al., 2009). The volumetric strength (Figure 1d) describes the resistance to isotropic deformation and, in the brittle layer, controls the formation of fluid-filled fractures such as dikes and sills (i.e., profiles V_1, V_2).

We define two main rheological test cases: TD—representing the Turkana Depression with a thin brittle layer and small Maxwell time corresponding to a weaker lithosphere (shear profile 1); and EP—representing the Ethiopian Plateau with a thick brittle layer and 100× higher Maxwell time (shear profile 2). Both have the volumetric strength profile V_1. Cases TD-V_2 and EP-V_2 are models with an increased elastic resistance to compaction (i.e., profile V_2). Magma transport vertically across the lithosphere is analyzed in a suite of 28 simulations that vary in terms of rheology, initial melt fraction $(\phi_{\max})$, and two boundary conditions: zero and non-zero tectonic extension rates typical of rifting (e.g., ~4 mm/yr (Knappe et al., 2020; Saria et al., 2014)). Simulations end when magma reaches the rock–air interface.

3. Magma Transport Under Zero and Non-Zero Tectonic Extension

Figure 2 shows model results with a low initial melt fraction $(\phi_{\max} = 0.5\%)$ and no tectonic extension (a) and with a background extensional strain rate of 10^{-16} s^{-1} (b). Top panels represent porosity, or the volume fraction of magma in the system, while the lower panels show accumulated plastic strain, or a measure of plastic deformation. Yellow dotted lines indicate the brittle–ductile transition, defined here as a change from dominantly elasto-plastic to dominantly viscous shear deformation (see Figure 3 for details). This transition also marks a change in melt transport and solid deformation, and confirms that case EP has a thicker brittle layer than case TD. The time required for magma to ascend to the surface in case EP (with a thicker brittle layer) is 4× less than for case TD under no tectonic extension; the cause of this difference is explored in the next section. This also holds for cases EP-V_2 and TD-V_2, but with only a 2× difference. The volumetric elastic strength promotes magma transport by opening tensile fractures more efficiently (i.e., case TD-V_2 is faster than case TD), but the effect is less clear when the shear strength is already more elastic (cases EP and EP-V_2).

The style of magma transport and solid deformation varies among the rheological cases. Roughly, the style of magma transport changes from porous and diapiric flow in the ductile regime to propagation of magma-filled fractures in the brittle regime (see Figure B1 in Supporting Information S1). This is marked by the dotted brittle–ductile transition. Cases TD and EP show a narrow magma conduit traversing the brittle layer vertically, interpreted as a dike. In contrast, V_2 cases display a widening of the melt body around 20 km depth (i.e., secondary melt reservoir), dominated by distributed plastic deformation, from which a shallow dike originates. In case TD, horizontal and vertical tensile fractures emerge from a region of higher melt fraction at the brittle–ductile transition, while in case EP, the horizontal fractures are diminished and strain is concentrated along the main vertical dike. Porosity waves, represented by thin fingers in the ductile layer, may form as a result of the visco-plastic compaction and de-compaction of the solid matrix, as described in previous models (e.g., Räss et al., 2019). In more elastic media, the porosity waves are diminished (cases EP and EP-V_2).

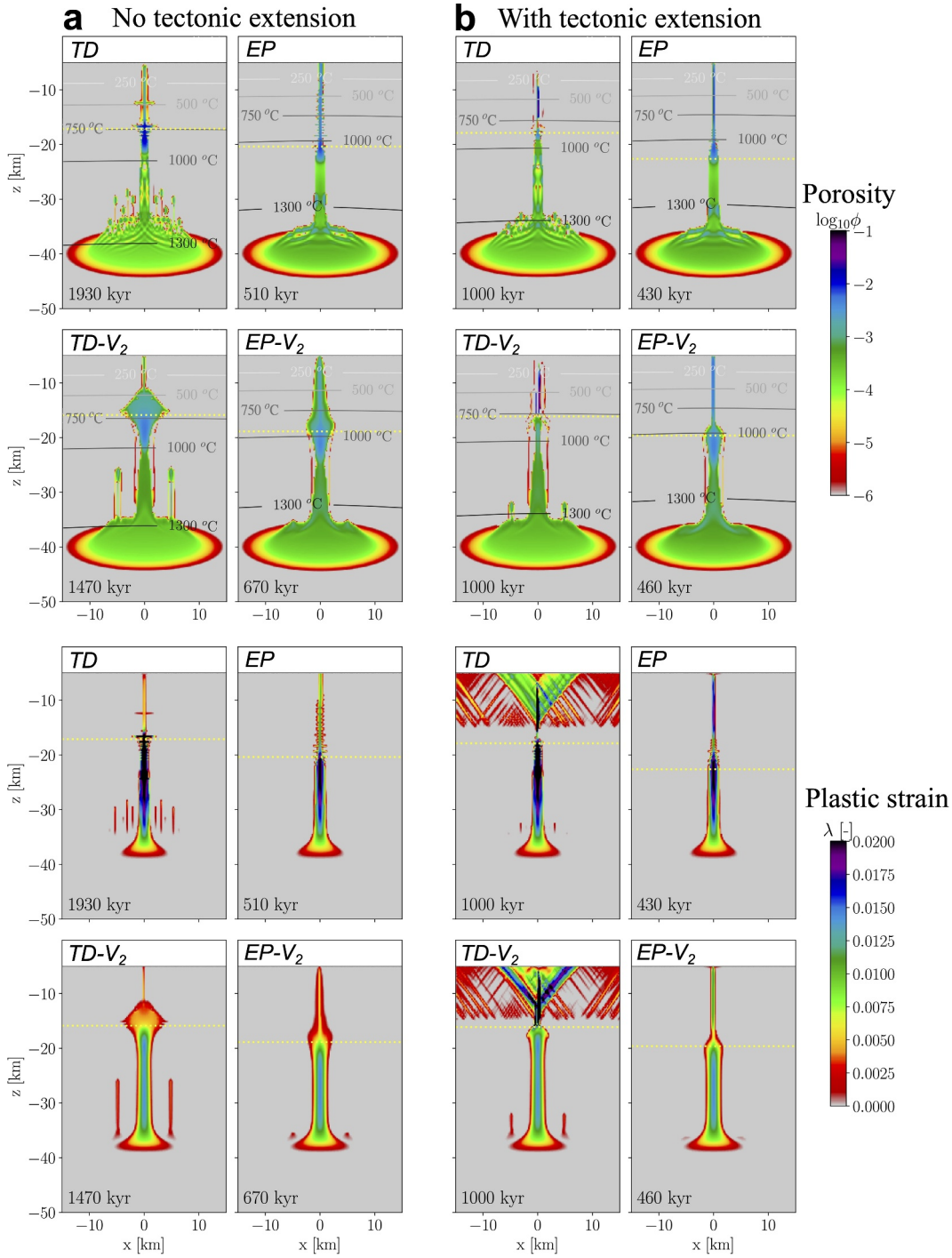

Figure 2. (a) Porosity and plastic strain maps for models with a low initial porosity $(\phi_{\max} = 0.5\%)$ and no extension. (b) Results of the same models with a background strain rate $\dot{\epsilon}_{BG} = 10^{-16}$ s^{-1}. Snapshots are shown when magma reached the rock–air interface. The dotted yellow lines represent the mechanical brittle–ductile transition detected at the tip of the rising magma body, and calculated as in Figure 3a. Cases: TD—Turkana Depression, EP—Ethiopian Plateau, and TD-V_2 and EP-V_2 are variations with volumetric strength profile V_2 shown in Figure 1d. Magma transport is faster in case EP compared to TD. In cases TD and TD-V_2, extension is partly accommodated in formation of shear zones, shown as regions of high plastic strain, while in cases EP and EP-V_2, all deformation is accommodated in diking. Plastic strain is calculated as the integral of plastic strain rate over time $\lambda = \int \dot{\lambda} dt$. Movies S1–S3 show the model evolution for cases TD and EP.

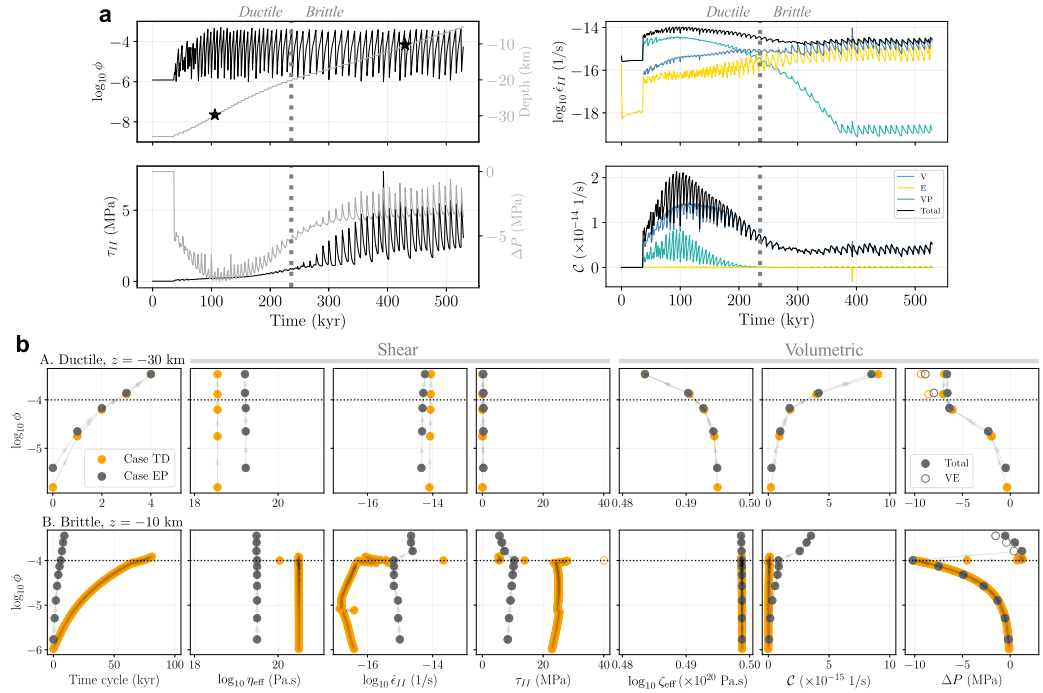

Figure 3. Deformation at the tip of the rising magma body. (a) Time evolution of parameters for case EP with a low initial porosity $(\phi_{\max} = 0.5\%)$ and no extension. From top to bottom, left to right: porosity, ϕ (black), depth (gray), the second invariant of shear stress, τ_{II} (black), phase pressure difference, ΔP (gray), shear strain rates, $\dot{\epsilon}_{II}$, and volumetric strain rates, $\mathcal{C}$. Abbreviations: V—viscous, E—elastic, VE—viscoelastic, and VP—viscoplastic. The brittle–ductile transition is shown with a dotted gray line and occurs when the viscous shear strain rates are equal to elastic shear strain rates (i.e., $\dot{\epsilon}_{II}^{V} = \dot{\epsilon}_{II}^{E}$). (b) Evolution of effective viscosities $(\eta_{\text{eff}}, \zeta_{\text{eff}})$, strain rates, and stresses in one failure cycle in the ductile (A) and brittle (B) regimes. The corresponding depths are shown with stars in panel (a) and each time increment is 1 kyr. η_{eff} and ζ_{eff} encompass our approach to model VE–VP rheology (see Supporting Information S1). The cycle has the following stages: magma recharge, shown as an increase in ϕ; plastic failure, manifested in a correction of VE stresses when Terzaghi's principle is reached $\phi \geq \phi_{\text{Tz}}, \phi_{\text{Tz}} = 10^{-4}$; and a gradual stress drop modulated by viscoplasticity when $\phi > \phi_{\text{Tz}}$. The failure cycle duration controls the magma ascent rate, with faster ascent rates due to shorter cycles.

Tectonic extension promotes magma ascent in all cases (i.e., faster ascent times, Figure 2b). In cases TD and TD-V_2, the strain is partly accommodated by deformation along shear zones in the brittle layer (i.e., mixed magmatic-tectonic extension). Diking-induced localization of shear zones can also be seen in these models. In cases EP and EP-V_2, all strain is accommodated by vertical dike propagation (i.e., fully magmatic extension). Simulation results with a higher initial melt fraction $(\phi_{\max} = 5\%)$ are shown in Figure B2 in Supporting Information S1.

4. Deformation at the Tip of a Rising Magma Body

To investigate how rock rheology impacts magma transport, we analyze the deformation at the tip of the rising magma body in each simulation. The tip is represented by the topmost grid cell that contains non-zero porosity ($\phi > 0$), and it is analogous to a fracture tip in most cases. The evolution of porosity, stresses, and strain rates at the tip are shown in Figure 3a for reference case EP with no tectonic extension. The brittle–ductile transition is marked by the thick dotted gray line and occurs when the elastic shear-strain rates are equal to the viscous shear-strain rates ($\dot{\epsilon}_{II}^{V} = \dot{\epsilon}_{II}^{E}$, intersection of yellow and cyan curves). The oscillations represent cycles of magma recharge and plastic failure caused by the application of Terzaghi's principle (Figure 3b). The evolution around a cycle is the following: As magma from below approaches the tip, there is a build-up of liquid overpressure (negative ΔP) and, to a lesser extent, shear stresses (larger τ_{II}). Once $\phi \geq \phi_{\text{Tz}}$, the rock contains sufficient melt that Terzaghi's principle is applied and the effective normal stress is reduced by the pore pressure. This reduction is enough to reach the failure criterion, leading to plastic failure at the tip, stress drop (i.e., correction of the

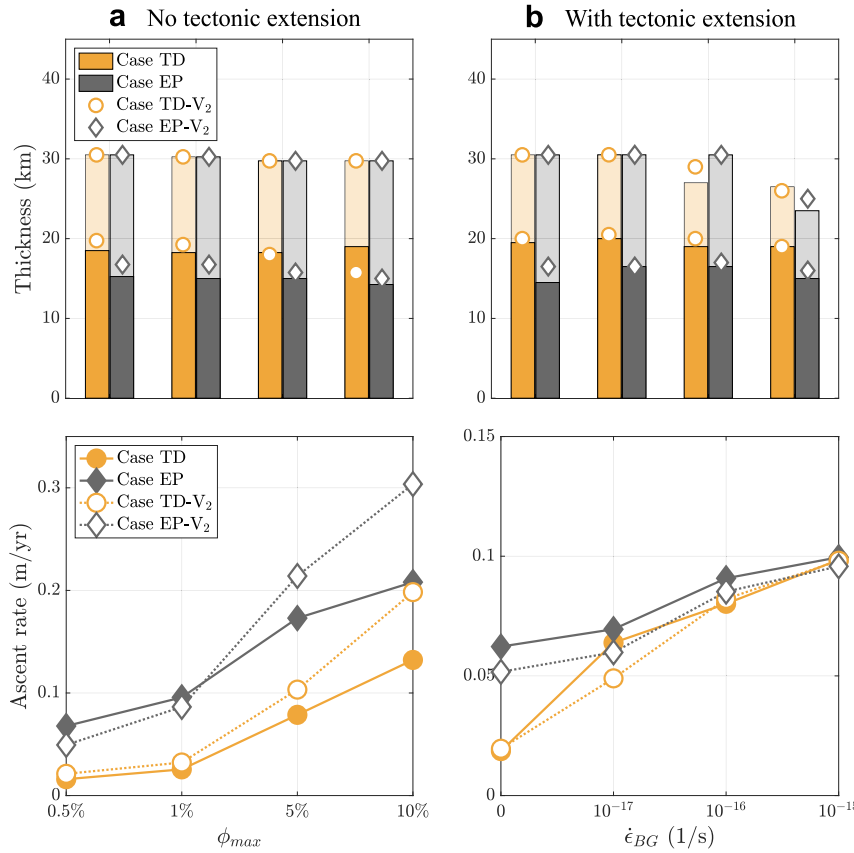

Figure 4. Rates of magma extraction for varying initial porosity $\phi_{\max}$ and no tectonic extension (a), and varying background strain rate $\dot{\epsilon}_{BG}$ for fixed $\phi_{\max} = 0.5\%$ (b). Top panels represent thickness of the ductile (solid) and brittle (transparent) layers calculated relative to the brittle–ductile transition (Figure 3a); bottom panels represent total ascent rates over the entire lithospheric column for the four rheological test cases. Each marker represents one simulation. Ascent rates are consistently faster for case EP with a thicker brittle layer despite the increase due to melt fraction (i.e., higher melt fraction increases buoyancy of magma). Extension facilitates magma extraction. The differences between rheological test cases are, however, reduced at higher extension rates.

viscoelastic stresses τ_{II}, ΔP), and transport of magma upwards. The faster the recharge of magma, the shorter the failure cycle and faster tip propagation.

Figure 3b compares the failure cycle in the ductile (dominantly viscous deformation, $z = -30$ km) and brittle (dominantly elastic deformation, $z = -10$ km) regimes for cases TD and EP. Each marker has a time increment of 1 kyr. The volumetric stresses for both TD and EP follow a similar evolution because both have V_1 volumetric strength profile (i.e., material parameters as shown in Figure 1d) and the failure cycles are evaluated at the same depths. In contrast, differences in cycle evolution between TD and EP are controlled by shear deformation. At low shear stresses, the ductile cycle is short due to a weaker matrix (lower effective viscosities $\eta_{\text{eff}}, \zeta_{\text{eff}}$) that, for a given stress, deforms at higher strain rates. Volumetric viscoplastic failure in the ductile regime may occur, which enables magma transport into zero permeability areas. The cycle duration and ascent rates are similar between cases TD and EP in the ductile regime.

In the brittle regime, the shear resistance is greater (higher effective viscosities) and requires larger stresses to deform the matrix. Case EP, however, has a slightly lower η_{eff} corresponding to a high Maxwell time, which translates into higher strain rates and liquid flux from below (Figure B3 in Supporting Information S1). In this case, the tip builds liquid overpressure fast and can fail earlier. For case TD, it is the opposite; a higher η_{eff} leads to large shear dissipation and slow magma supply from below. Brittle cycles are 8–10 times longer than EP, with large shear stress drops of ~20 MPa during failure. However, as shown previously, the overall slowdown of TD

relative to EP is only 4× because of a thick ductile layer with faster ascent rates and a thin brittle layer with slow rates.

All simulations are summarized in Figure 4, which shows the thickness of the ductile (solid) and brittle (transparent) layers and total ascent rates for varying initial porosity (a) and background strain rate (b). For zero tectonic extension, ascent rates increase with the initial melt fraction $\phi_{\max}$ (Figure 4a). This is expected; with increasing melt fraction, magma has more buoyancy and can rise at faster rates. Nonetheless, the contrast between TD and EP remains significant at all melt fractions. Case TD is consistently slower despite having a thinner brittle layer. The faster ascent rates in case EP derive from transport in the brittle layer (Figure B5 in Supporting Information S1). Figure 4b shows that extension promotes magma extraction in all cases. However, the differences between cases TD and EP are reduced considerably at high extension rates, meaning that extension effects supersede the rheological behavior.

5. Discussion and Conclusions

Results indicate that magma extraction is faster across a thick, brittle layer (case EP, large Maxwell time) than across a thin, weakened layer (case TD, small Maxwell time). The differences arise from the solid deformation at the tip of the rising magma body, and are controlled by the rheological mode and tectonic extension. Additional experiments show sensitivity of results to model parameters (Figure B6 in Supporting Information S1). In particular, results are sensitive to the plasticity formulation (i.e., the reduction of viscoplastic regularization viscosity, Li et al. (2023)), but counter-intuitively, with accelerated magma extraction in case EP and slowdown to complete arrest of magma below the brittle layer in case TD. Our models, therefore, support the hypothesis that the thinned and weakened lithosphere beneath Turkana acted as a barrier for melt transport. This provides an explanation for the sporadic magmatism observed in Turkana over the last 30 Myr compared to the neighboring plateaus.

A scenario in which the lithosphere beneath Turkana has been weakened by either multiple rifting episodes and/or magmatic intrusions is also in agreement with previous models used to explain the diffuse faulting (Brune et al., 2017; Buck, 1991; Corti et al., 2019). With the onset of rifting, Figure 2b shows that case TD develops into a mixed magmatic–tectonic mode in which extension is accommodated by both dike intrusion and distributed fault slip. In contrast, case EP may become fully magmatic under extension, analogous to a narrow, magma-rich rift architecture. Our study differs from previous work that considered simple melt pathways—dikes cutting the entire lithosphere (Buck, 2006). Instead, complex melt pathways may form depending on melt availability and the thermo-mechanical state of the lithosphere (Figure 2 and Figure B2 in Supporting Information S1). We also show that magma can intrude the crust and facilitate lithospheric extension without erupting. Thus, we explain why rifts may be magmatic and not volcanic, and how magma-assisted rifting may produce different outcomes. However, a common criticism of previous models is that they are unable to explain the diachronous evolution of magmatism and faulting in Turkana. Observations suggest that magmatism and sedimentary basins migrated from west to east in the last 25 Myr (e.g., Ebinger et al., 2000, and references therein). One explanation for the migration is that basal lithospheric topography channeled plume material and melts to surrounding regions (Ebinger & Sleep, 1998), although it is not obvious why melts would avoid areas of lithosphere thinning in Turkana. Alternatively, variations in lithospheric strength across the depression could account for the eastward migration (Morley, 1994). In either case, melt seems to have avoided the weakened, rifted zone in Turkana, including during the early Cenozoic flood-basalt phase (Hendrie et al., 1994; Morley, 1999; Steiner et al., 2022). A key prediction of our models is that rheologically weak structures in the lithosphere impact magma ascent pathways, and a variety of magmatic expressions may co-exist: isolated, sporadic volcanic centers, crustal intrusions, and lateral migration of magma to neighboring regions that allow more efficient extraction.

Current observations are not conclusive about the extent of magmatic intrusion and modification in the Turkana lithosphere and how these have varied over time. Low seismic $V_p/V_s \approx 1.74$ ratios beneath Turkana argue against widespread and voluminous lower crustal intrusions (Kounoudis et al., 2023; Ogden et al., 2023). On the other hand, geochemical and geological data indicate periods of magmatism punctuated by volcanic hiatus, where magmas stall at medium to shallow crustal levels (Morley, 2020; Steiner et al., 2024). It is clear that melts may perturb the compositional and thermal structure of the lithosphere but how these processes are recorded in the observational data set remains to be explored.

Although we consider a single brittle–ductile transition and no compositional variations, we demonstrate the complex relationship between magma flux, the thermo-mechanical state of the lithosphere, and the rate of extension on the evolution of rift systems (e.g., Brune et al., 2023). In reality, the complex tectonic history in Turkana has given rise to significant variations in the rheological structure of the lithosphere (Ebinger et al., 2000). Musila et al. (2023) identified two present-day regions of contrasting rift architecture in the depression: northern Turkana, in which the deformation style is diffuse across an ∼300 km-wide seismically active zone spanning older rifts; and southern Turkana, which is in a state of incipient magmatic strain localization (Knappe et al., 2020; Muirhead et al., 2022; Ogden et al., 2023; Rooney et al., 2022). Our hypothesis seems more applicable to the northern Turkana, while southern Turkana represents an intermediate case. It has also been proposed that the plume head associated with the early flood-basalt magmatism dissipated before the onset of rifting, such that the Turkana lithosphere has largely cooled and is rather strong, despite the permanent crustal thinning (Kounoudis et al., 2023; Ogden et al., 2023). If this hypothesis is correct, future models will have to provide a better explanation for the diffuse magmatism and deformation.

In summary, our models suggest that the rheological mode and thickness of the lithosphere exert a counter-intuitive control on melt extraction, which can explain the unusual pattern of volcanism and faulting in the Turkana Depression. This has implications for understanding the coupled magmatic–tectonic history of rifting, but also more broadly, the relationship between melt extraction and crustal thickness (e.g., Bonnet Gibet et al., 2022).

Data Availability Statement

The melt extraction model is implemented in the code `morfault`, available at https://github.com/apusok/FD-PDE, directory `models/morfault`. The version of the code and input files to reproduce the results in this study is available at Pusok et al. (2025). The Supporting Information S1 contains information on theory, code implementation, model set-up, and additional results.

Acknowledgments
We thank R. Kounoudis and C. Ebinger for discussions, the editor F. Capitanio, and two anonymous reviewers for useful comments. This work was supported by the European Research Council (Horizon2020, #772255), the Royal Society (URF\R1\231613), and the National Science Foundation (EAR-2121568 and OAC-2311208). Numerical simulations were computed on the Arcus-C cluster, Advanced Research Computing, Oxford.

References

Albaric, J., Déverchère, J., Petit, C., Perrot, J., & Le Gall, B. (2009). Crustal rheology and depth distribution of earthquakes: Insights from the central and southern East African Rift System. *Tectonophysics*, *468*(1), 28–41. https://doi.org/10.1016/j.tecto.2008.05.021

Bastow, I. D., Pilidou, S., Kendall, J.-M., & Stuart, G. W. (2010). Melt-induced seismic anisotropy and magma assisted rifting in Ethiopia: Evidence from surface waves. *Geochemistry, Geophysics, Geosystems*, *11*(6), 1–12. https://doi.org/10.1029/2010GC003036

Benoit, M. H., Nyblade, A. A., & VanDecar, J. C. (2006). Upper mantle P-wave speed variations beneath Ethiopia and the origin of the Afar hotspot. *Geology*, *34*(5), 329–332. https://doi.org/10.1130/G22281.1

Bialas, R. W., Buck, W. R., & Qin, R. (2010). How much magma is required to rift a continent? *Earth and Planetary Science Letters*, *292*(1–2), 68–78. https://doi.org/10.1016/j.epsl.2010.01.021

Bonnet Gibet, V., Michaut, C., Wieczorek, M., & Lognonné, P. (2022). A positive feedback between crustal thickness and melt extraction for the origin of the Martian dichotomy. *Journal of Geophysical Research: Planets*, *127*(12), 1–28. https://doi.org/10.1029/2022JE007472

Boone, S. C., Seiler, C., Kohn, B. P., Gleadow, A. J. W., Foster, D. A., & Chung, L. (2018). Influence of rift superposition on lithospheric response to East African Rift System extension: Lapur range, Turkana, Kenya. *Tectonics*, *37*(1), 182–207. https://doi.org/10.1002/2017TC004575

Boyce, A., Bastow, I. D., Cottar, S., Kounoudis, R., Guilloud De Courbeville, J., Caunt, E., & Desai, S. (2021). AFRP20: New P-wavespeed model for the African mantle reveals two whole-mantle plumes below East Africa and neoproterozoic modification of the Tanzania Craton. *Geochemistry, Geophysics, Geosystems*, *22*(3), 1–27. https://doi.org/10.1029/2020GC009302

Brune, S., Corti, G., & Ranalli, G. (2017). Controls of inherited lithospheric heterogeneity on rift linkage: Numerical and analog models of interaction between the Kenyan and Ethiopian rifts across the Turkana depression. *Tectonics*, *36*(9), 1767–1786. https://doi.org/10.1002/2017TC004739

Brune, S., Kolawole, F., Olive, J., Stamps, D., Buck, W., Buiter, S., et al. (2023). Geodynamics of continental rift initiation and evolution. *Nature Reviews Earth & Environment*, *4*, 235–253. https://doi.org/10.1038/s43017-023-00391-3

Buck, W. R. (1991). Modes of continental lithospheric extension. *Journal of Geophysical Research*, *96*(B12), 20161–20178. https://doi.org/10.1029/91JB01485

Buck, W. R. (2004). Consequences of asthenospheric variability on continental rifting. In G. Karner, B. Taylor, & D. Kohlstedt (Eds.), *Rheology and deformation of the lithosphere at continental margins* (pp. 1–31). Columbia University Press. https://doi.org/10.7312/karn12738-002

Buck, W. R. (2006). The role of magma in the development of the Afro-Arabian Rift System. *Geological Society, London, Special Publications*, *259*(1), 43–54. https://doi.org/10.1144/GSL.SP.2006.259.01.05

Chambers, E. L., Harmon, N., Rychert, C. A., Gallacher, R. J., & Keir, D. (2022). Imaging the seismic velocity structure of the crust and upper mantle in the northern East African Rift using Rayleigh wave tomography. *Geophysical Journal International*, *230*(3), 2036–2055. https://doi.org/10.1093/gji/ggac156

Cornwell, D. G., Mackenzie, G. D., England, R. W., Maguire, P. K. H., Asfaw, L. M., & Oluma, B. (2006). Northern Main Ethiopian Rift crustal structure from new high-precision gravity data. *Geological Society, London, Special Publications*, *256*(1), 307–321. https://doi.org/10.1144/gsl.sp.2006.259.01.23

Corti, G. (2009). Continental rift evolution: From rift initiation to incipient break-up in the Main Ethiopian Rift, East Africa. *Earth-Science Reviews*, *96*(1), 1–53. https://doi.org/10.1016/j.earscirev.2009.06.005

Corti, G., Cioni, R., Franceschini, Z., Sani, F., Scaillet, S., Molin, P., et al. (2019). Aborted propagation of the Ethiopian rift caused by linkage with the Kenyan rift. *Nature Communications*, *10*(1), 1–11. https://doi.org/10.1038/s41467-019-09335-2

Courtillot, V., Jaupart, C., Manighetti, I., Tapponnier, P., & Besse, J. (1999). On causal links between flood basalts and continental breakup. *Earth and Planetary Science Letters*, *166*(3), 177–195. https://doi.org/10.1016/S0012-821X(98)00282-9

Craig, T. J., & Jackson, J. A. (2021). Variations in the seismogenic thickness of East Africa. *Journal of Geophysical Research: Solid Earth*, *126*(3), 1–15. https://doi.org/10.1029/2020JB020754

Davidson, A., & Rex, D. C. (1980). Age of volcanism and rifting in southwestern Ethiopia. *Nature*, *283*(5748), 657–658. https://doi.org/10.1038/283657a0

Ebinger, C. J., & Casey, M. (2001). Continental breakup in magmatic provinces: An Ethiopian example. *Geology*, *29*(6), 527–530. https://doi.org/10.1130/0091-7613(2001)029⟨0527:CBIMPA⟩2.0.CO;2

Ebinger, C. J., Deino, A. L., Drake, R. E., & Tesha, A. L. (1989). Chronology of volcanism and rift basin propagation: Rungwe volcanic province, East Africa. *Journal of Geophysical Research*, *94*(B11), 15785–15803. https://doi.org/10.1029/JB094iB11p15785

Ebinger, C. J., & Ibrahim, A. (1994). Multiple episodes of rifting in central and East Africa: A re-evaluation of gravity data. *Geologische Rundschau*, *83*(4), 689–702. https://doi.org/10.1007/BF00251068

Ebinger, C. J., & Sleep, N. (1998). Cenozoic magmatism throughout East Africa resulting from impact of a single plume. *Nature*, *395*(6704), 788–791. https://doi.org/10.1038/27417

Ebinger, C. J., Yemane, T., Harding, D. J., Tesfaye, S., Kelley, S., & Rex, D. C. (2000). Rift deflection, migration, and propagation: Linkage of the Ethiopian and Eastern rifts, Africa. *GSA Bulletin*, *112*(2), 163–176. https://doi.org/10.1130/0016-7606(2000)112⟨163:RDMAPL⟩2.0.CO;2

Erbello, A., Colleps, C., Melnick, D., Sobel, E. R., Bookhagen, B., Pingel, H., et al. (2024). Magma-assisted continental rifting: The broadly rifted zone in SW Ethiopia, East Africa. *Tectonics*, *43*, 1–26. https://doi.org/10.1029/2022TC007651

Furman, T., Kaleta, K. M., Bryce, J. G., & Hanan, B. B. (2006). Tertiary mafic lavas of Turkana, Kenya: Constraints on East African plume structure and the occurrence of high-volcanism in Africa. *Journal of Petrology*, *47*(6), 1221–1244. https://doi.org/10.1093/petrology/egl009

George, R., Rogers, N., & Kelley, S. (1998). Earliest magmatism in Ethiopia: Evidence for two mantle plumes in one flood basalt province. *Geology*, *26*(10), 923–926. https://doi.org/10.1130/0091-7613(1998)026⟨0923:EMIEEF⟩2.3.CO;2

Global Volcanism Program. (2013). *Volcanoes of the world (v. 4.8.7)*. Smithsonian Institution. https://doi.org/10.5479/si.GVP.VOTW4-2013

Hendrie, D. B., Kusznir, N. J., Morley, C. K., & Ebinger, C. J. (1994). Cenozoic extension in northern Kenya: A quantitative model of rift basin development in the Turkana region. *Tectonophysics*, *236*(1–4), 409–438. https://doi.org/10.1016/0040-1951(94)90187-2

Kendall, J.-M., & Lithgow-Bertelloni, C. (2016). Why is Africa rifting? *Geological Society, London, Special Publications*, *420*(1), 11–30. https://doi.org/10.1144/SP420.17

Kendall, J.-M., Pilidou, S., Keir, D., Bastow, I. D., Stuart, G. W., & Ayele, A. (2006). Mantle upwellings, melt migration and the rifting of Africa: Insights from seismic anisotropy. *Geological Society, London, Special Publications*, *259*, 271–272. https://doi.org/10.1144/GSL.SP.2006.259.01.06

Knappe, E., Bendick, R., Ebinger, C. J., Birhanu, Y., Lewi, E., Floyd, M., et al. (2020). Accommodation of East African rifting across the Turkana depression. *Journal of Geophysical Research: Solid Earth*, *125*(2), 1–13. https://doi.org/10.1029/2019JB018469

Kounoudis, R., Bastow, I. D., Ebinger, C. J., Darbyshire, F., Ogden, C. S., Musila, M., et al. (2023). The development of rifting and magmatism in the multiply rifted Turkana Depression, East Africa: Evidence from surface-wave analysis of crustal and uppermost mantle structure. *Earth and Planetary Science Letters*, *621*, 118386. https://doi.org/10.1016/j.epsl.2023.118386

Kounoudis, R., Bastow, I. D., Ebinger, C. J., Ogden, C. S., Ayele, A., Bendick, R., et al. (2021). Body-wave tomographic imaging of the Turkana Depression: Implications for rift development and plume-lithosphere interactions. *Geochemistry, Geophysics, Geosystems*, *22*(8), 1–27. https://doi.org/10.1029/2021GC009782

Li, Y., Davis, T., Pusok, A. E., & Katz, R. F. (2025). Models of buoyancy-driven dykes using continuum plasticity and fracture mechanics: A comparison. *Geoscientific Model Development, EGUsphere*, 1–33. https://doi.org/10.5194/egusphere-2024-3504

Li, Y., Pusok, A. E., Davis, T., May, D., & Katz, R. F. (2023). Continuum approximation of dyking with a theory for poro-viscoelastic–viscoplastic deformation. *GJI*, *234*(3), 2007–2031. https://doi.org/10.1093/gji/ggad173

Lin, S.-C., Kuo, B.-Y., Chiao, L.-Y., & van Keken, P. E. (2005). Thermal plume models and melt generation in East Africa: A dynamic modeling approach. *Earth and Planetary Science Letters*, *237*(1–2), 175–192. https://doi.org/10.1016/j.epsl.2005.04.049

Mechie, J., Keller, G. R., Prodehl, C., Gaciri, S., Braile, L. W., Mooney, W. D., et al. (1994). Crustal structure beneath the Kenya rift from axial profile data. *Tectonophysics*, *236*(1–4), 179–200. https://doi.org/10.1016/0040-1951(94)90176-7

Mechie, J., Keller, G. R., Prodehl, C., Khan, M. A., & Gaciri, S. J. (1997). A model for the structure, composition and evolution of the Kenya rift. *Tectonophysics*, *278*(1–4), 95–119. https://doi.org/10.1016/S0040-1951(97)00097-8

Morley, C. K. (1994). Interaction of deep and shallow processes in the evolution of the Kenya rift. *Tectonophysics*, *236*(1), 81–91. https://doi.org/10.1016/0040-1951(94)90170-8

Morley, C. K. (1999). Influence of preexisting fabrics on rift structure. In C. K. Morley (Ed.), *Geoscience of rift systems—evolution of East Africa* (pp. 1–20). American Association of Petroleum Geologists. https://doi.org/10.1306/St44623C9

Morley, C. K. (2020). Early syn-rift igneous dike patterns, northern Kenya rift (Turkana, Kenya): Implications for local and regional stresses, tectonics, and magma-structure interactions. *Geosphere*, *16*(3), 890–918. https://doi.org/10.1130/GES02107.1

Morley, C. K., Wescott, W., Stone, D., Harper, R., Wigger, S., & Karanja, F. (1992). Tectonic evolution of the northern Kenyan rift. *Journal of the Geological Society*, *149*(3), 333–348. https://doi.org/10.1144/gsjgs.149.3.033

Moucha, R., & Forte, A. (2011). Changes in African topography driven by mantle convection. *Nature Geoscience*, *4*(10), 707–712. https://doi.org/10.1038/ngeo1235

Muirhead, J., Scholz, C., & Rooney, T. (2022). Transition to magma-driven rifting in the south Turkana basin: Part I. *Journal of the Geological Society*, *179*(6), 1–15. https://doi.org/10.1144/jgs2021-159

Musila, M., Ebinger, C. J., Bastow, I. D., Sullivan, G., Oliva, S. J., Knappe, E., et al. (2023). Active deformation constraints on the Nubia-Somalia plate boundary through heterogenous lithosphere of the Turkana Depression. *Geochemistry, Geophysics, Geosystems*, *24*(9), 1–26. https://doi.org/10.1029/2023GC010982

Ogden, C. S., Bastow, I. D., Ebinger, C., Ayele, A., Kounoudis, R., Musila, M., et al. (2023). The development of multiple phases of superposed rifting in the Turkana Depression, East Africa: Evidence from receiver functions. *Earth and Planetary Science Letters*, *609*, 118088. https://doi.org/10.1016/j.epsl.2023.118088

Oliva, S. J., Ebinger, C. J., Wauthier, C., Muirhead, J. D., Roecker, S. W., Rivalta, E., & Heimann, S. (2019). Insights into fault-magma interactions in an early-stage continental rift from source mechanisms and correlated volcano-tectonic earthquakes. *Geophysical Research Letters*, *46*(4), 2065–2074. https://doi.org/10.1029/2018GL080866

Pérez-Gussinyé, M., Metois, M., Fernández, M., Vergés, J., Fullea, J., & Lowry, A. R. (2009). Effective elastic thickness of Africa and its relationship to other proxies for lithospheric structure and surface tectonics. *Earth and Planetary Science Letters*, *287*(1), 152–167. https://doi.org/10.1016/j.epsl.2009.08.004

Pik, R., Marty, B., & Hilton, D. (2006). How many mantle plumes in Africa? The geochemical point of view. *Chemical Geology*, *226*(3–4), 100–114. https://doi.org/10.1016/j.chemgeo.2005.09.016

Pusok, A. E., Katz, R. F., May, D. A., & Li, Y. (2022). Chemical heterogeneity, convection and asymmetry beneath mid-ocean ridges. *Geophysical Journal International*, *231*(3), 2055–2078. https://doi.org/10.1093/gji/ggac309

Pusok, A. E., Li, Y., May, D., & Katz, R. (2025). FD-PDE framework, morfault: v1.1.0 [Software]. *Zenodo*. https://doi.org/10.5281/zenodo.15297276

Rajaonarison, T. A., Stamps, D. S., Naliboff, J., Nyblade, A., & Njinju, E. A. (2023). A geodynamic investigation of plume-lithosphere interactions beneath the East African Rift. *Journal of Geophysical Research: Solid Earth*, *128*(4), 1–22. https://doi.org/10.1029/2022JB025800

Räss, L., Duretz, T., & Podladchikov, Y. (2019). Resolving hydromechanical coupling in two and three dimensions: Spontaneous channelling of porous fluids owing to decompaction weakening. *Geophysical Journal International*, *218*(3), 1591–1616. https://doi.org/10.1093/gji/ggz239

Ritsema, J., Deuss, A., van Heijst, H. J., & Woodhouse, J. H. (2011). S40RTS: A degree-40 shear-velocity model for the mantle from new Rayleigh wave dispersion, teleseismic traveltime and normal-mode splitting function measurements. *Geophysical Journal International*, *184*(3), 1223–1236. https://doi.org/10.1111/j.1365-246X.2010.04884.x

Rogers, N., Macdonald, R., Fitton, J. G., George, R., Smith, M., & Barreiro, B. (2000). Two mantle plumes beneath the East African rift system: Sr, Nd and Pb isotope evidence from Kenya rift basalts. *Earth and Planetary Science Letters*, *176*(3–4), 387–400. https://doi.org/10.1016/S0012-821X(00)00012-1

Rooney, T. O. (2017). The cenozoic magmatism of east-Africa: Part I — Flood basalts and pulsed magmatism. *Lithos*, *286–287*, 264–301. https://doi.org/10.1016/j.lithos.2017.05.014

Rooney, T. O. (2020). The cenozoic magmatism of East Africa: Part III – Rifting of the craton. *Lithos*, *360*, 105390. https://doi.org/10.1016/j.lithos.2020.105390

Rooney, T. O., Herzberg, C., & Bastow, I. D. (2012). Elevated mantle temperature beneath East Africa. *Geology*, *40*(1), 27–30. https://doi.org/10.1130/G32382.1

Rooney, T. O., Wallace, P. J., Muirhead, J. D., Chiasera, B., Steiner, R. A., Girard, G., & Karson, J. A. (2022). Transition to magma-driven rifting in the south Turkana basin: Part 2. *Journal of the Geological Society*, *179*(6), 1–19. https://doi.org/10.1144/jgs2021-160

Saria, E., Calais, E., Stamps, D. S., Delvaux, D., & Hartnady, C. J. H. (2014). Present-day kinematics of the East African Rift. *Journal of Geophysical Research: Solid Earth*, *119*(4), 3584–3600. https://doi.org/10.1002/2013JB010901

Stamps, D. S., Flesch, L. M., Calais, E., & Ghosh, A. (2014). Current kinematics and dynamics of Africa and the East African Rift System. *Journal of Geophysical Research: Solid Earth*, *119*(6), 5161–5186. https://doi.org/10.1002/2013JB010717

Steiner, R. A., Rooney, T. O., Girard, G., Rogers, N., Ebinger, C. J., Peterson, L., & Phillips, R. K. (2022). Initial cenozoic magmatic activity in East Africa: New geochemical constraints on magma distribution within the eocene continental flood basalt province. In R. K. Srivastava, R. E. Ernst, K. L. Buchan, & M. de Kock (Eds.), *Large igneous provinces and their plumbing systems* (pp. 435–465). Geological Society, London, Special Publications. https://doi.org/10.1144/SP518-2020-262

Steiner, R. A., Rooney, T. O., Kappelman, J., Lydic, T., Girard, G., Mariita, N., & Phillips, R. (2024). Messengers from the magma Chambers: Petrostratigraphic analysis of plagioclase-rich flood basalt lavas in Turkana, Kenya. *Journal of Petrology*, *65*(6), 1–21. https://doi.org/10.1093/petrology/egae044

Terzaghi, K. (1943). *Theoretical soil mechanics* (1st ed.). John Wiley & Sons. https://doi.org/10.1002/9780470172766

Tiberi, C., Gautier, S., Ebinger, C. J., Roecker, S., Plasman, M., Albaric, J., et al. (2019). Lithospheric modification by extension and magmatism at the craton-orogenic boundary: North Tanzania Divergence, East Africa. *Geophysical Journal International*, *216*(3), 1693–1710. https://doi.org/10.1093/gji/ggy521

References From the Supporting Information

Balay, S., Abhyankar, S., Adams, M. F., Brown, J., Brune, P., Buschelman, K., et al. (2019). *PETSc users manual. Technical Report ANL-95/11 - Revision 3.12*. Argonne National Laboratory. Retrieved from https://www.mcs.anl.gov/petsc

Biot, M. (1941). General theory of three dimensional consolidation. *Journal of Applied Physics*, *12*(2), 155–164. https://doi.org/10.1063/1.1712886

Chevalier, L., & Schmeling, H. (2022). Thermal non-equilibrium of porous flow in a resting matrix applicable to melt migration: A parametric study. *Solid Earth*, *13*(6), 1045–1063. https://doi.org/10.5194/se-13-1045-2022

Connolly, J. A. D., & Podladchikov, Y. (1998). Compaction-driven fluid flow in viscoelastic rock. *Geodinamica Acta*, *11*(2–3), 55–84. https://doi.org/10.1080/09853111.1998.11105311

Crameri, F., Schmeling, H., Golabek, G. J., Duretz, T., Orendt, R., Buiter, S. J. H., et al. (2012). A comparison of numerical surface topography calculations in geodynamic modelling: An evaluation of the "sticky air" method. *Geophysical Journal International*, *189*(1), 38–54. https://doi.org/10.1111/j.1365-246X.2012.05388.x

Duretz, T., Räss, L., de Borst, R., & Hageman, T. (2023). A comparison of plasticity regularization approaches for geodynamic modeling. *Geochemistry, Geophysics, Geosystems*, *24*(7), 1–19. https://doi.org/10.1029/2022GC010675

Gerya, T. (2010). Dynamical instability produces transform faults at mid-ocean ridges. *Science*, *329*(5995), 1047–1050. https://doi.org/10.1126/science.1191349

Harlow, F. H., & Welch, J. E. (1965). Numerical calculation of time-dependent viscous incompressible flow of fluid with free surface. *The Physics of Fluids*, *8*(2182), 1–8. https://doi.org/10.1063/1.1761178

Katz, R. F. (2022). *The dynamics of partially molten rock* (1st ed.). Princeton Univ. Press.

Keller, T., May, D. A., & Kaus, B. (2013). Numerical modelling of magma dynamics coupled to tectonic deformation of lithosphere and crust. *Geophysical Journal International*, *195*(3), 1406–1442. https://doi.org/10.1093/gji/ggt306

McKenzie, D. (1984). The generation and compaction of partially molten rock. *Journal of Petrology*, *25*(3), 713–765. https://doi.org/10.1093/petrology/25.3.713

Minarik, W. G., & Bruce Watson, E. (1995). Interconnectivity of carbonate melt at low melt fraction. *Earth and Planetary Science Letters*, *133*(3–4), 423–437. https://doi.org/10.1016/0012-821X(95)00085-Q

Rasolofosaon, P. N. J., & Zinszner, B. E. (2009). Poroelastic equations closely examined by ultrasonic experiments in rocks. In H. I. Ling, A. Smyth, & R. Betti, (Eds.) *Poromechanics IV: Proceedings of the fourth biot conference on poromechanics* (pp. 661–666).

Rudge, J. F. (2018). Textural equilibrium melt geometries around tetrakaidecahedral grains. *Proceedings of the Royal Society A: Mathematical, Physical and Engineering Sciences A.*, *474*(2212), 1–24. https://doi.org/10.1098/rspa.2017.0639

Schmeling, H., Marquart, G., & Grebe, M. (2018). A porous flow approach to model thermal non-equilibrium applicable to melt migration. *Geophysical Journal International*, *212*(1), 119–138. https://doi.org/10.1093/gji/ggx406

Tan, X., & Konietzky, H. (2014). Numerical study of variation in Biot's coefficient with respect to microstructure of rocks. *Tectonophysics*, *610*, 159–171. https://doi.org/10.1016/j.tecto.2013.11.014

Tian, D., Uieda, L., Leong, W. J., Fröhlich, Y., Schlitzer, W., Grund, M., et al. (2024). PyGMT: A Python interface for the generic mapping tools. https://doi.org/10.5281/zenodo.11062720

Wark, D. A., & Watson, E. B. (1998). Grain-scale permeabilities of texturally equilibrated, monomineralic rocks. *Earth and Planetary Science Letters*, *164*(3–4), 591–605. https://doi.org/10.1016/S0012-821X(98)00252-0